

On the optimum shape of thin adhesive strips for various peeling directions

Janine C. Mergel, Roger A. Sauer¹

Graduate School AICES, RWTH Aachen University, Templergraben 55, 52056 Aachen, Germany

Published² in *The Journal of Adhesion*, DOI: [10.1080/00218464.2013.840538](https://doi.org/10.1080/00218464.2013.840538)

Submitted on 23 July 2013, Revised on 06 August 2013, Accepted on 30 August 2013

Abstract: This work studies optimal shapes of peeling films considering different peeling directions. A cohesive zone model is used to capture normal and tangential forces during peeling. The strip is modeled by nonlinear finite elements based on geometrically exact beam theory. Criteria for optimization are proposed that account for the strain energy during deformation, the overall peeling energy, and the maximum peeling forces. These criteria are first analyzed for various test geometries and then considered for computational optimization. Two cases are considered: Optimization for single direction and optimization for multiple directions. The latter allows the determination of strip shapes that provide strong attachment and easy detachment under different peeling angles.

Keywords: computational shape optimization, adhesive tapes, cohesive zone models, peeling angle, gecko adhesion

1 Introduction

Flexible and strongly adhesive structures that are easily removable from the substrate are important for many applications, such as the fabrication of reusable adhesive tapes or the adhesion mechanisms of various insects and lizards. Hence they have been subject of numerous investigations. The anisotropic attachment and detachment behavior of the microstructures underneath gecko toes, for instance, has been investigated by many researchers, e.g. by Autumn et al. [2, 1], Tian et al. [16], Chen et al. [4] and Zhao et al. [18, 19].

One of the most widely used approaches for studying direction-dependent peeling of thin strips is to consider the analytical model of Kendall [6], see e.g. [4, 3]. The Kendall model however, does not account for the bending stiffness and the shear flexibility of the peeling strip.

To understand and improve the adhesion properties of thin adhesives, the influence of the shape on the peeling behavior has been investigated for vertical peeling both theoretically [14, 13, 5] and numerically [15, 8, 7]. Silves et al. [15], for instance, have designed the width and the adhesion distribution of thin beams for a prescribed force-displacement dependence, using topology optimization. Recently, Mergel et al. [7] have proposed essential criteria and guidelines for the shape optimization of adhesive microstructures. They have performed both a detailed benchmark study and computational optimization for different parameters. In both studies, however, the authors have considered only a perpendicular peeling direction. The main purpose of this paper is therefore

¹Corresponding author, email: sauer@aices.rwth-aachen.de, phone: +49 241 80-99129

²This pdf is the personal version of an article whose final publication is available at www.tandfonline.com.

1. To investigate the optimum shape of thin and flexible structures that can resist large external peeling forces for various peeling directions and
2. to obtain strongly adhesive strips that can be released easily for a certain direction.

Since the structures considered here are thin and elongated, we model the peeling strip as a beam, using the beam formulation of Sauer and Mergel [12]. The adhesion between the strip and a rigid, planar substrate is modeled by a cohesive zone model. In general, the formulation considered here can be used for applications of arbitrary dimension, e.g. for the shape optimization of structures at both the nano-scale or macro-scale. One very promising application is the optimization of bio-inspired adhesives based on the adhesion mechanisms of insects and lizards. This, however, is outside the scope of the current work. Here, our aim is rather to provide an insight into optimum shapes for directional peeling in general.

The remaining sections of this paper are structured as follows: Section 2 briefly outlines the beam model equations and the shape optimization problem considered here. The peeling behavior of different test geometries is discussed in Section 3. Section 4 presents peeling strip geometries obtained from computational optimization. Section 5 finally concludes this paper.

2 Modeling

This section discusses the problem setup and summarizes the governing equations describing the mechanical behavior of the peeling strip. We define the contact formulation applied for the interaction between the strip and the substrate. Afterwards, we provide the criteria and constraints of the considered optimization problem. For a numerical solution the resulting equations are discretized within a finite element framework, which is not discussed here. See [12, 7] for a more detailed derivation.

2.1 Setup

The thin strip that we are investigating here has length L and a rectangular cross-section. Its height $H(S)$ and width $B(S)$ may vary along $S \in [0, L]$. The right part of the strip with length L_c adheres to a planar and rigid substrate. Figure 1 shows the peeling strip in the initial configuration. Since the thickness of the strip is considerably smaller than its length we

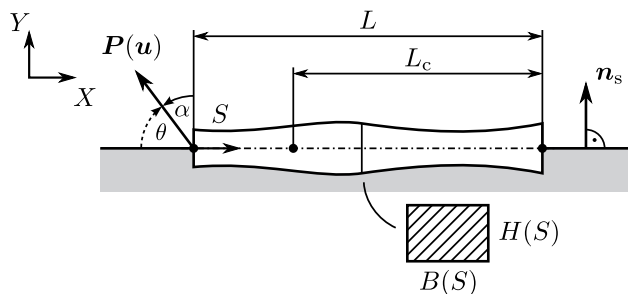


Figure 1: Initial configuration of the peeling strip.

consider, for the sake of simplicity, the beam axis as initially straight.³ The strip is peeled from the substrate by prescribing a displacement \mathbf{u} with magnitude $u := \|\mathbf{u}\|$ at the left boundary.

³We assume that the arising error is small compared to the approximation error of beam theory.

As shown in the figure, the resulting reaction force $\mathbf{P}(\mathbf{u})$ is inclined from the surface normal of the substrate, \mathbf{n}_s , by the angle α , i.e.

$$\mathbf{P} \cdot \mathbf{n}_s = P \cdot \cos \alpha, \quad P := \|\mathbf{P}\|, \quad \alpha \in [-90^\circ, 90^\circ]. \quad (1)$$

We note that studies based on the Kendall model usually consider the peeling angle $\theta = 90^\circ - \alpha$, see the figure. Since we want to preserve the positive sense of rotation in the (X, Y) -plane, however, we use α in the following.

2.2 Balance of work

For the peeling strip we use the two-dimensional beam formulation of Sauer and Mergel [12]. This formulation, which is only outlined here, is based on the geometrically exact theory by Reissner [9]. It accounts for finite deformation and strains due to elongation, bending, and shearing of the beam. For a prescribed displacement, \mathbf{u} , the balance of work is given in incremental form by

$$d\Pi_{\text{int}} + d\Pi_c - d\Pi_{\text{ext}} = 0, \quad (2)$$

see e.g. [10, 12]. Here, $d\Pi_{\text{int}}$ denotes the internal energy due to elastic beam deformation, $d\Pi_c$ the contact energy, and $d\Pi_{\text{ext}}$ the externally applied work. The three terms are given by [12]

$$d\Pi_{\text{int}} = \int_L d\boldsymbol{\varepsilon}^T \mathbf{D} \boldsymbol{\varepsilon} dS, \quad d\Pi_c = - \int_L d\mathbf{d}^T \begin{bmatrix} \mathbf{T}_c \\ M_c \end{bmatrix} B dS, \quad d\Pi_{\text{ext}} = \mathbf{P}(\mathbf{u}) \cdot d\mathbf{u}, \quad (3)$$

where \mathbf{d} contains the X - and Y -displacements and the rotation of the beam section plane, and $\boldsymbol{\varepsilon}$ is composed of the axial, shear, and bending strains. Considering a linear elastic material behavior with Young's modulus, E , and a shear modulus, G , we obtain for the material tensor $\mathbf{D} = \text{diag}(EA, GA_s, EI)$. The area, A , effective shear area, A_s , and second moment of area, I , are given for a rectangular beam cross-section by $A = HB$, $A_s = 5/6 A$, and $I = 1/12 H^3 B$ [12]. The following section defines the contact traction, \mathbf{T}_c , and the distributed contact moment, M_c , that act at every point on the beam axis along L .

2.3 Contact formulation

Recently, Mergel et al. [7] have used a van der Waals adhesion model in order to optimize the shape of thin strips peeled perpendicularly from a substrate. The model considered in that study, however, does not account for tangential contact. It is therefore not suitable for modeling peeling in any other than the normal direction of the substrate surface. In order to include tangential contact, we apply the exponential cohesive zone model (CZM) by Xu and Needleman [17] here, see also [11, 12],

$$\mathbf{T}_{\text{CZM}} = \begin{cases} -\frac{T_0}{g_0} \exp\left(1 - \frac{\|\mathbf{g}_s\|}{g_0}\right) \mathbf{g}_s & \text{for } S \in [L - L_c, L], \\ \mathbf{0} & \text{for } S \in [0, L - L_c], \end{cases} \quad (4)$$

where T_0 and g_0 are cohesion parameters. As we consider an initially straight beam axis for this study, we simplify the model provided by Sauer and Mergel [12] by applying the cohesive forces directly at the axis instead of the lower strip surface. The contact forces hence do not cause any bending moment, i.e. $M_c = 0$. The gap vector, \mathbf{g}_s , contains the X - and Y -displacements of the beam axis, which correspond to the first two entries of \mathbf{d} . Since \mathbf{T}_{CZM} acts in the direction $-\mathbf{g}_s$, Eq. (4) incorporates both normal and tangential contact.

We note that formulation (4) is unstable in compression [12]. As we further want to avoid that the non-adhesive part of the strip is pressed into the substrate, we consider an additional penalty force with penalty parameter ε for the entire beam,

$$\mathbf{T}_{\text{pen}} = \begin{cases} \varepsilon g_N^2 \mathbf{n}_s, & g_N < 0, \\ \mathbf{0}, & g_N \geq 0 \end{cases} \quad \text{for } S \in [0, L], \quad (5)$$

where

$$g_N = \mathbf{g}_s \cdot \mathbf{n}_s \quad (6)$$

is the signed normal gap between the beam axis and the substrate surface. We thus have

$$\mathbf{T}_c = \mathbf{T}_{\text{CZM}} + \mathbf{T}_{\text{pen}}, \quad M_c = 0. \quad (7)$$

2.4 Shape optimization

In [7] we have considered for the shape optimization of strongly adhesive and flexible strips

1. the maximization of the externally applied work, Π_{ext} ,
2. the maximization of the total contact energy, Π_c^∞ , and
3. the minimization of the peak internal energy during peeling, $\Pi_{\text{int}}^{\text{max}}$.

The first two criteria, however, have been recognized to be nearly equivalent [7]. We consider for this reason the second and third criteria, and maximize in addition the maximum of the peeling force,

$$P_{\text{max}} = \max_{\mathbf{u}} \|\mathbf{P}\|. \quad (8)$$

The peak internal energy and the total contact energy can be obtained by [7]

$$\Pi_{\text{int}}^{\text{max}} = \max_{\mathbf{u}} \Pi_{\text{int}} \quad \text{and} \quad \Pi_c^\infty = w_{\text{CZM}}^\infty A_c, \quad A_c = \int_{L_c} B \, dS, \quad (9)$$

where w_{CZM}^∞ is the contact energy per unit area, which is required for full separation. It can be computed by integrating $\|\mathbf{T}_{\text{CZM}}\|$ in Eq. (4) from $\|\mathbf{g}_s\| = 0$ to $\|\mathbf{g}_s\| = \infty$, i.e. [12]

$$w_{\text{CZM}}^\infty = T_0 g_0 \exp(1). \quad (10)$$

Both P_{max} and $\Pi_{\text{int}}^{\text{max}}$ depend on the peeling angle, α , while Π_c^∞ is a function only of the strip width. We consider in the following two different objective functions to be minimized. To obtain strong peeling resistance in direction of α , we consider an objective function very similar to the one provided by Mergel et al. [7],

$$\Psi_1(\alpha) = \frac{c_p}{\overline{P}_{\text{max}}(\alpha)} + \overline{\Pi}_{\text{int}}^{\text{max}}(\alpha) + \frac{c_c}{\overline{\Pi}_c^\infty}. \quad (11)$$

The overbar indicates that the corresponding variable is normalized with a chosen reference variable, i.e. $\overline{(\bullet)} = (\bullet) / (\bullet)^{\text{ref}}$. The minimization of Ψ_1 results in a large maximum peeling force and contact area but small deformation energy during peeling. The three criteria can be weighted by varying the parameters c_p and c_c , where $c_p, c_c \geq 0$ are chosen constants.⁴ For the sake of simplicity, we use $c_p = c_c = 1$ here. A detailed investigation of c_p and c_c for vertical

⁴If $c_\bullet = 0$, the corresponding term is omitted; if $c_\bullet \rightarrow \infty$, the term is weighted most strongly.

peeling, considering the external energy instead of the maximum peeling force, can be found in [7].

It is important for many applications that the peeling strip does not only adhere strongly for a certain peeling direction but can also be removed easily in another direction. One well-known example is the direction dependency of the gecko adhesion mechanism, see e.g. [2, 1]. We thus consider a second objective function, which maximizes the peeling force for the angle α_{\max} but minimizes the force for a different angle, α_{\min} ,

$$\Psi_2(\alpha_{\max}, \alpha_{\min}) = \left[\frac{c_p^{\max}}{\bar{P}_{\max}(\alpha_{\max})} + c_p^{\min} \bar{P}_{\max}(\alpha_{\min}) \right] + [\bar{\Pi}_{\text{int}}^{\max}(\alpha_{\max}) + \bar{\Pi}_{\text{int}}^{\max}(\alpha_{\min})] + \frac{c_c}{\bar{\Pi}_c^{\infty}}, \quad (12)$$

where c_p^{\max} , c_p^{\min} , $c_c \geq 0$. In conclusion, we formulate the following problem statement, considering the optimization constraints suggested by Mergel et al. [7]:

Problem statement

Find $H(S)$, $B(S)$, $S \in [0, L]$, such that Ψ_1 or Ψ_2 is minimized subject to the constraints

- 1) $V \leq V_{\max}$ for the beam volume $V = \int_L HB \, dS$,
- 2) $H(S) \in [H_{\min}, H_{\max}]$, $B(S) \in [B_{\min}, B_{\max}]$,
- 3) $|\partial^2 H / \partial S^2| \leq H''_{\max}$, $|\partial^2 B / \partial S^2| \leq B''_{\max}$, and
- 4) the peeling process is quasi-static.

Constraints 1) – 3) are restrictions on the geometry of the peeling strip. According to 1), the structure must not exceed a maximum permitted volume. We further prescribe intervals for the admissible height and width, which is referred to as box constraint, and restrict the second derivatives of $H(S)$ and $B(S)$.

3 Peeling study of differently shaped test geometries

This section discusses the direction-dependent peeling behavior of a set of differently shaped test geometries. We consider linear functions for the height and width of the peeling strip in order to study the optimization criteria of Eq. (11) and (12).

3.1 Strip geometry

We combine three functions F_{incr} , F_{const} , and F_{decr} to describe both the strip height or width,

$$F_{\text{incr}}(S) = c_F + d_F \cdot (S - 0.5L), \quad (13)$$

$$F_{\text{const}}(S) = c_F, \quad (14)$$

$$F_{\text{decr}}(S) = c_F - d_F \cdot (S - 0.5L), \quad (15)$$

$F = H, B$, and $S \in [0, L]$. We thus obtain nine different shapes, see Figure 2a. The curve parameters, c_H , c_B , d_H , and d_B , are chosen such that all strips have an equal volume. We consider 75% of the strip as adhesive, i.e. $L_c = 0.75L$. All geometry, material, and cohesion parameters can be found in Table 5.

We now investigate different peeling directions, α . An angle of $\alpha = 0^\circ$ corresponds to peeling in vertical direction. We note that linear functions for H and B have been considered in a previous benchmark study for vertical peeling as well [7]. Nevertheless, the present work includes this peeling case for the sake of completeness due to differences in the chosen geometry parameters, the applied contact formulation, and the optimization criteria. For an angle of $\alpha = 90^\circ$, the strip is purely elongated by pulling its tip sideward. If $\alpha \approx -90^\circ$, the tip is also pulled sideward but in the opposite direction. Depending on the relation between the beam stiffness and the cohesion strength, the strip may be bent strongly during peeling. The case $\alpha = -90^\circ$, for which the beam would be compressed along its beam axis, is not considered here because we do not investigate strip buckling in this study. To avoid buckling it is sufficient, however, to vary the angle slightly by choosing e.g. $\alpha = -89^\circ$.

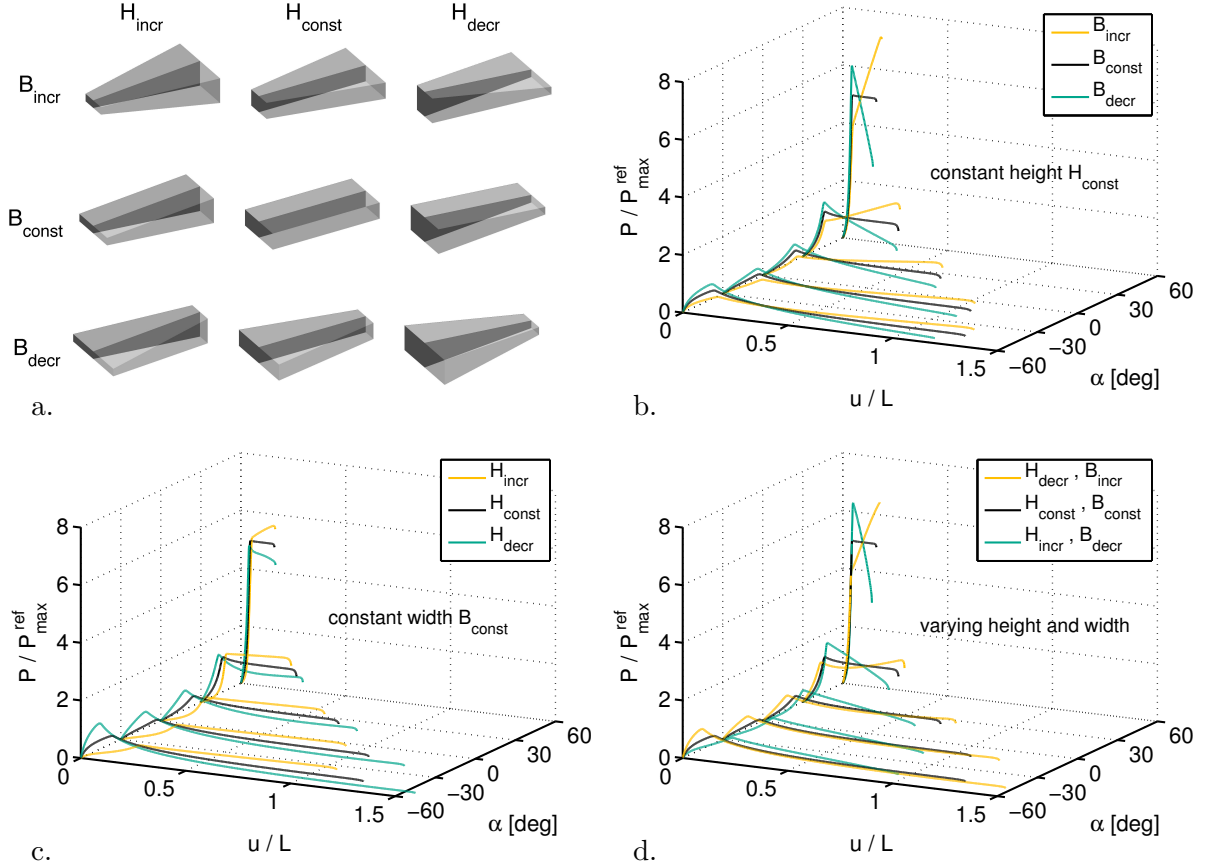


Figure 2: Test geometries with constant / linear height, H , and width, B : a. Illustration of the shapes (exaggerated), the left boundary is peeled from the substrate; b. – d. Normalized peeling force for different peeling angles, α ; b. Variation of B (middle column of a.); c. Variation of H (middle row of a.); d. Combination of increasing H (or B) and decreasing B (or H).

3.2 Peeling behavior

In the following, we examine the maximum force, P_{max} , the maximum internal energy, $\Pi_{\text{int}}^{\text{max}}$, and the total contact energy, Π_c^∞ . Therefore we use the values obtained with shape ($H_{\text{const}}, B_{\text{const}}$) for normalization, see Table 6 in the appendix. Figures 2b – 2d compare the force-displacement relations of different test geometries for $\alpha \in [-60^\circ, 60^\circ]$. Table 1 shows the maximum peeling reaction forces for $\alpha \in [-89^\circ, 90^\circ]$.

$P_{\max}/P_{\max}^{\text{ref}}$		-89°	-60°	-45°	-30°	0°	30°	45°	60°	90°
H_{incr}	B_{incr}	1.24	1.12	1.13	1.20	1.57	2.73	4.27	7.91	23.54
H_{const}	B_{incr}	0.90	0.69	0.72	0.81	1.17	2.24	3.69	7.14	20.05
H_{decr}	B_{incr}	1.86	1.09	0.96	0.91	0.98	1.86	3.24	6.42	15.76
H_{incr}	B_{const}	0.80	0.73	0.75	0.80	1.07	1.89	2.98	5.60	16.47
H_{const}	B_{const}	1.23	0.90	0.84	0.84	1.00	1.66	2.61	4.99	13.62
H_{decr}	B_{const}	2.22	1.29	1.13	1.07	1.16	1.72	2.57	4.82	15.02
H_{incr}	B_{decr}	1.05	0.91	0.91	0.95	1.23	2.16	3.42	6.31	15.43
H_{const}	B_{decr}	1.56	1.11	1.03	1.02	1.21	1.98	3.12	6.02	16.64
H_{decr}	B_{decr}	2.40	1.42	1.25	1.19	1.30	1.97	2.97	5.70	17.76

Table 1: Normalized maximum peeling force for the considered test geometries varying the peeling angle, α ; the smallest and largest value are marked in bold.

		Π_c/Π_c^{ref}	$\Pi_{\text{int}}^{\max}/\Pi_{\text{int}}^{\text{ref}}$				
			-45°	-30°	0°	30°	45°
H_{incr}	B_{incr}	1.13	2.91	2.53	1.92	1.63	2.00
H_{const}	B_{incr}	1.13	2.18	1.89	1.40	1.08	1.22
H_{decr}	B_{incr}	1.13	1.47	1.32	1.03	0.74	0.76
H_{incr}	B_{const}	1.00	2.25	1.95	1.45	1.07	1.06
H_{const}	B_{const}	1.00	1.57	1.37	1.00	0.71	0.69
H_{decr}	B_{const}	1.00	1.08	1.00	0.84	0.66	0.58
H_{incr}	B_{decr}	0.88	1.57	1.38	1.04	0.73	0.65
H_{const}	B_{decr}	0.88	1.20	1.10	0.90	0.69	0.59
H_{decr}	B_{decr}	0.88	0.93	0.88	0.79	0.67	0.61

Table 2: Maximum internal energy for different peeling angles, α , and total contact energy, considering the nine test geometries; the optimum values are marked in bold.

Initially, the reaction force builds up rapidly for all considered shapes, see Figures 2b – 2d. During this phase the entire adhesive part still remains attached to the substrate. The actual beginning of the peeling can be observed as a kink in the force-displacement curves of Figure 2. We denote the corresponding force required to start the peeling process build-up force here. This force becomes larger if α increases from 0° to 90° , regardless of the strip geometry. If the angle is negative, the build-up force first decreases but becomes larger again if α approximates -90° , see also Table 1. This phenomenon is probably caused by the finite bending resistance of the considered peeling strip, which becomes most apparent for $\alpha \ll 0^\circ$.

After reaching the build-up force, the slope of the reaction force, $\partial P/\partial u$, is larger for $\partial B/\partial S > 0$ than for $\partial B/\partial S = 0$, and smaller for $\partial B/\partial S < 0$, see Figure 2b. This agrees well with observations made by Pantano et al. [8] and Mergel et al. [7]. Figure 2c shows that, for the parameters considered here, the same effect occurs for $\partial H/\partial S > 0$ and $\partial H/\partial S < 0$. We observe that the higher the angle, α , the stronger is the influence of the slopes of H and B on the force.

Figure 3 compares exemplarily all strip shapes for two different angles, $\alpha = 0^\circ$ (solid line) and $\alpha = -45^\circ$ (dashed line). It is seen from Figure 3 and from Figure 2d that the curve of the peeling force strongly depends on the relation between H and B and on the peeling direction. We can thus not assume that the build-up force is the maximum force if the structure is shaped arbitrarily. We further observe that for the strips with constant width (black line), the maximum force is larger for the decreasing height H_{decr} (Figure 3b) than for both H_{incr} (Figure 3a) and H_{const} (Figure 3c). This phenomenon has been reported by Pantano et al. [8] but has not been

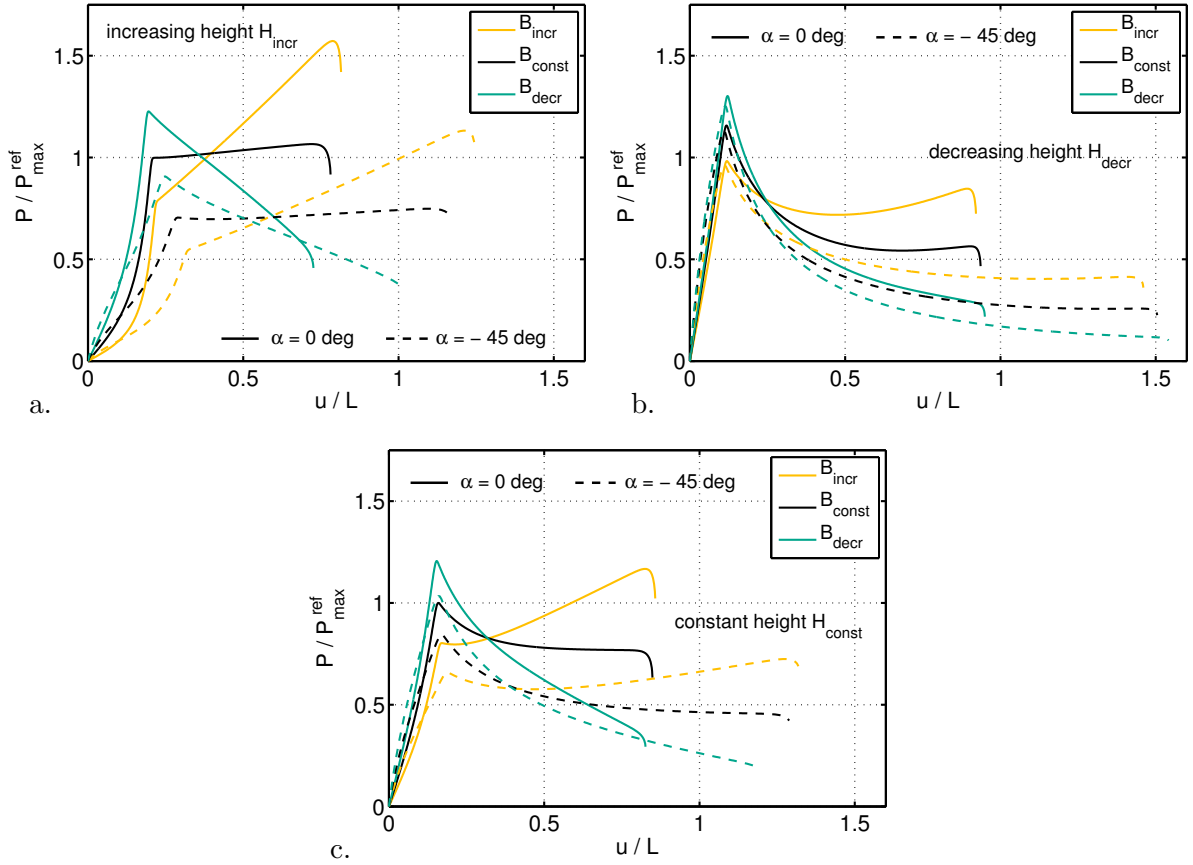


Figure 3: Comparison of the force-displacement relations for the peeling angles $\alpha = 0^\circ$ (solid line) and $\alpha = -45^\circ$ (dashed line): a. Test geometries with increasing height (left column of Fig. 2a); b. Test geometries with decreasing height (right column of Fig. 2a); c. Test geometries with constant height (middle column of Fig. 2a).

observed by Mergel et al. [7] for the geometry and material parameters considered in [7]. This is discussed further in Section 3.4.

As Table 2 shows, the contact energy is largest for geometries with increasing width, $B = B_{\text{incr}}$. The deformation minimizes for strips that become thinner towards their tip, $H = H_{\text{decr}}$. This agrees with the results for $\alpha = 0^\circ$, considering van der Waals adhesion [7]. Figure 4 shows the objective function, Ψ_1 , evaluated for the nine geometries and for different peeling angles. The location of the minimum of Ψ_1 is circled. Towards $\alpha \in \{-45^\circ, -30^\circ, 0^\circ\}$, the geometries $(H_{\text{decr}}, B_{\text{decr}})$ and $(H_{\text{decr}}, B_{\text{const}})$ are rated best, probably due to their small deformation energy, $\Pi_{\text{int}}^{\text{max}}$, but large maximum force, P_{max} . For $\alpha = \{30^\circ, 45^\circ\}$ and the parameters considered here, $(H_{\text{decr}}, B_{\text{incr}})$ and $(H_{\text{incr}}, B_{\text{const}})$ have the smallest costs, Ψ_1 . Figure 5 shows Ψ_2 for two different combinations of peeling directions, $(45^\circ, -45^\circ)$ and $(30^\circ, -30^\circ)$. We observe that for these cases, the cost, Ψ_2 is minimal for shape $(H_{\text{decr}}, B_{\text{const}})$.

In fact, the detachment behavior of thin strips is affected by several other parameters beside their thickness or width, which are not investigated in this study. It has been shown, for instance, that the peeling force depends on both the ratio L_c/L [7] and the relation between the material stiffness and the adhesion strength [10]. It is further assumed that the strip length, L , compared to the range of adhesion may have influence [7].

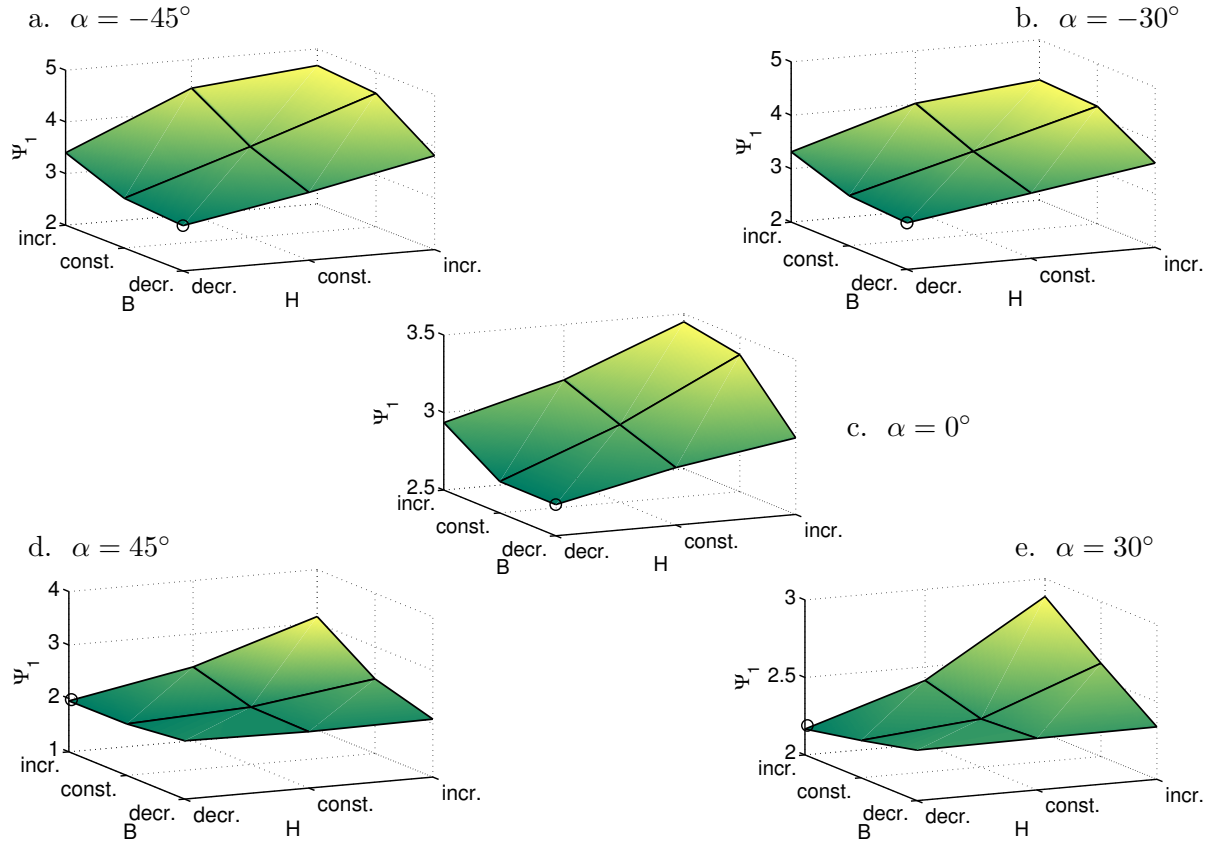


Figure 4: Objective function Ψ_1 (single peeling direction) for the test geometries, considering $c_p = 1$, $c_c = 1$ and different peeling angles, $\alpha \in [-45^\circ, 45^\circ]$; the minimum of Ψ_1 is circled.

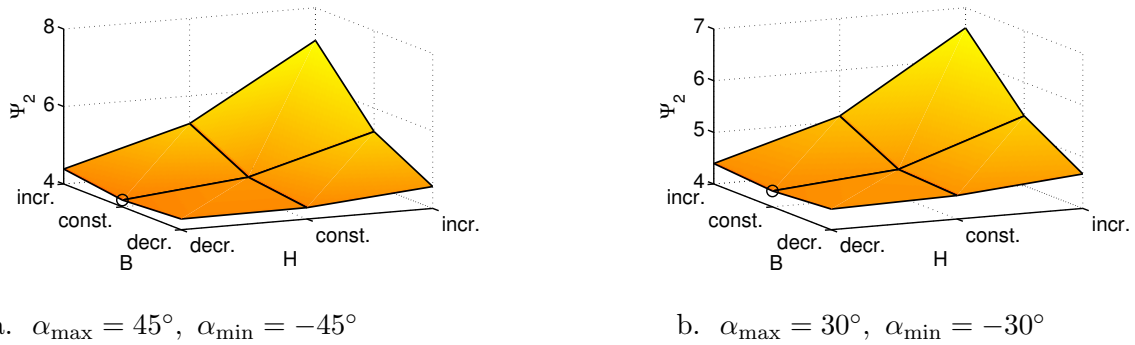


Figure 5: Objective function Ψ_2 (multiple peeling directions) for the test geometries, considering $c_p^{\max} = c_p^{\min} = 1$, $c_c = 1$ and different peeling angles, $\alpha_{\max}, \alpha_{\min} \in [-45^\circ, 45^\circ]$; the minimum of Ψ_2 is circled.

3.3 Comparison with the Kendall model

A common approach for investigating directional peeling of thin strips is to consider the analytical peeling model of Kendall [6]. This model considers the deformation of a strip with a constant height and width due to pure elongation. We compare the peeling behavior of the test geometry ($H_{\text{const}}, B_{\text{const}}$) with the Kendall model, keeping in mind that the applied computational beam model also accounts for the bending resistance and the shear flexibility of the beam. Those are both neglected in the Kendall model. The required force for a certain peeling direction can be computed for the Kendall model by

$$\frac{P_K}{EBH} = \sqrt{[1 - \cos \theta]^2 + 2 \frac{w_{\text{CZM}}^\infty}{EH}} - [1 - \cos \theta], \quad \theta = 90^\circ - \alpha, \quad (16)$$

see e.g. [10].

Figure 6a shows the relative error between the Kendall force and the maximum peeling force from the beam model. The deformation of the beam axis shortly before detachment and the deformation of a Kendall strip are shown for various peeling angles in Figure 6b. As one can see in the figures, the results agree well only for $\alpha = 90^\circ$ ($\theta = 0^\circ$), where the error is less than 0.01%. This coincides with the assumption that the strip deforms due to pure elongation in this case. The smaller the peeling angle, however, the larger is the relative error between both solutions, over 20% for vertical peeling, and nearly 70% for $\alpha = -89^\circ$. The remarkable differences are to be expected due to the strong bending deformation of the peeling strip, see Figure 6b, which has been reported by Sauer [10], considering vertical peeling. This phenomenon cannot be accounted for with the peeling model of Kendall. Furthermore, it is seen in Figures 2 and 3 that the assumption of a constant reaction force during peeling is valid for bending-resistant strips only if

1. they have a constant height and width and
2. they are deformed by pure elongation, i.e. $\alpha = 90^\circ$.

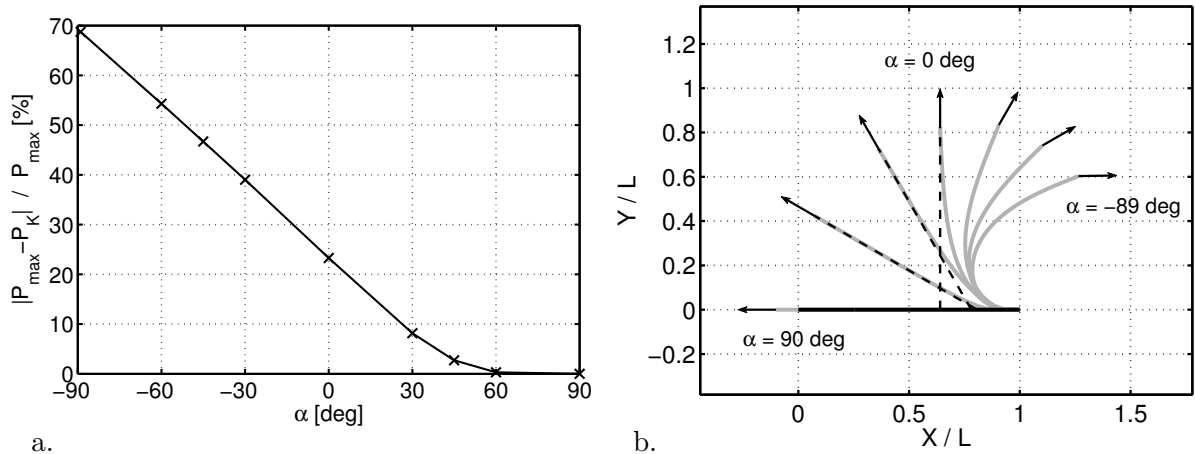


Figure 6: Peeling behavior of geometry ($H_{\text{const}}, B_{\text{const}}$) according to the beam model in comparison to the peeling model of Kendall [6]: a. Relative error between the maximum peeling force and the Kendall force for different peeling directions, α ; b. Deformation of the beam axis shortly before full detachment.

3.4 Modified strip height

Motivated by the results discussed in Section 3.2, we now investigate how a slightly modified strip height influences the peeling behavior. We consider for this purpose a peeling strip with constant width, B_{const} , peeled vertically from the substrate, i.e. $\alpha = 0^\circ$. As Figure 7a shows, its non-adhesive part has a constant thickness, H_{const} , while the height increases / decreases linearly at the adhesive part, $S \in [L - L_c, L]$. We denote the thickness of the right tip as H_{tip} here. The other parameters correspond to those used in Section 3.2, see Table 5. Figure 7b shows the force-displacement relation for different tip heights. The black curve belongs to geometry $(H_{\text{const}}, B_{\text{const}})$. The maximum peeling force in dependence of the ratio $H_{\text{tip}} / H_{\text{const}}$ is shown in Figure 7c. One can see from Figures 7b and 7c that the relation between the maximum force and the slope $\partial H / \partial S$ is strongly non-linear. For the parameters considered

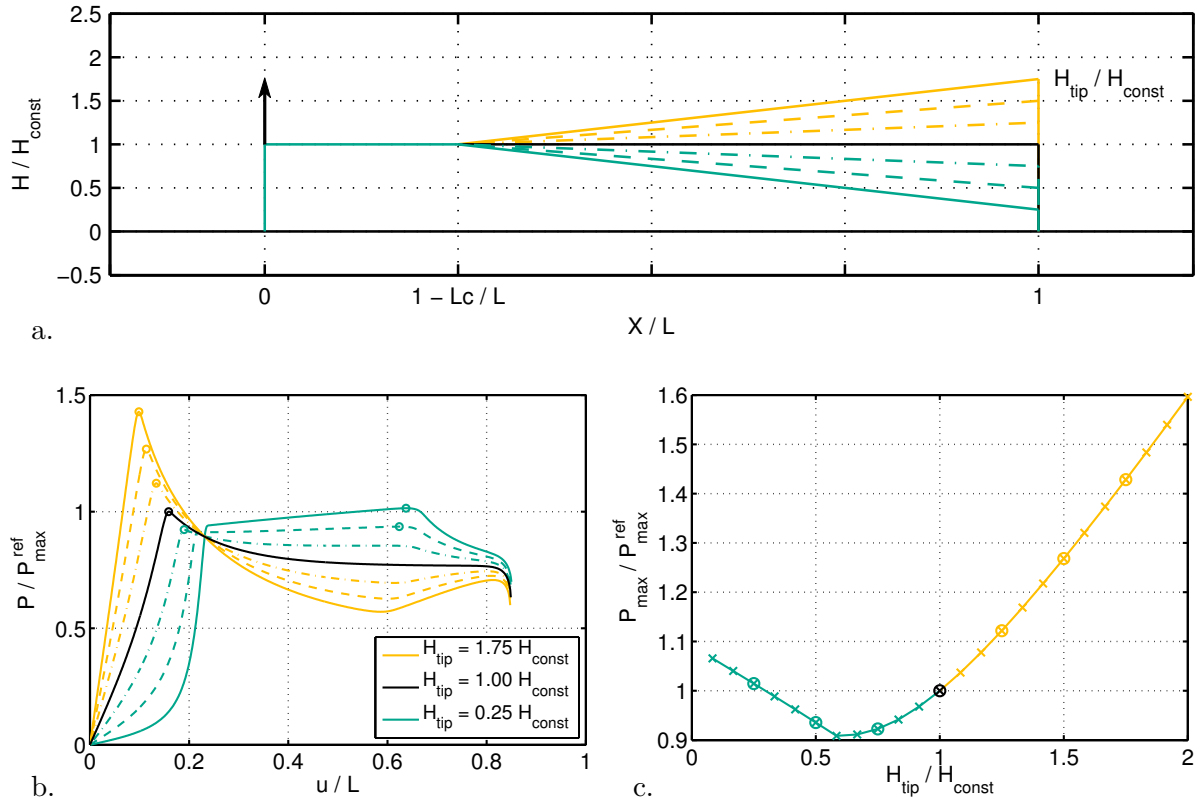


Figure 7: Peeling behavior of a strip with constant width, B_{const} , and varying tip height, H_{tip} : a. Normalized strip height; b. Force-displacement relation for $\alpha = 0^\circ$; c. Normalized maximum peeling force for $\alpha = 0^\circ$, the maximum values shown in b. are marked with a circle.

here, P_{max} reaches its minimum for the tip height $H_{\text{tip}}^{\text{min}} \approx 0.583 H_{\text{const}}$, where the peeling force remains nearly constant after building up. If $H_{\text{tip}} < H_{\text{tip}}^{\text{min}}$, P_{max} increases linearly with decreasing tip height. We can conclude from the comparison of $H_{\text{tip}} = 0.25 H_{\text{const}}$ (green blue solid line), $1 H_{\text{const}}$ (black line), and $1.75 H_{\text{const}}$ (orange solid line) that the maximum force can be increased not only by an increasing but also by a decreasing strip height, which may explain the differences in the observations of Pantano et al. [8] and Mergel et al. [7].

4 Computational shape optimization of peeling strips

After investigating the directional peeling of prescribed test shapes in Section 3, we now consider computational shape optimization based on the algorithm of Mergel et al. [7]. We note that, in general, it cannot be guaranteed to find the absolute minimum for non-convex optimization problems. We refer to [7] for a detailed discussion of the applied algorithm.

4.1 Single peeling direction

First, we maximize the peeling force along a certain peeling direction, i.e. we minimize $\Psi_1(\alpha)$ in Eq. (11) for different angles, $\alpha \in [-45^\circ, 45^\circ]$. The parameters considered here are given in Table 7. Figure 8 shows the optimum shape of the peeling strips that we obtain with shape optimization for different directions. For -45° and -30° , the peeling strip is very thick at the non-adhesive part, but flattens at the adhesive part. We observe from Table 3 that both geometries attained the maximum permitted volume.

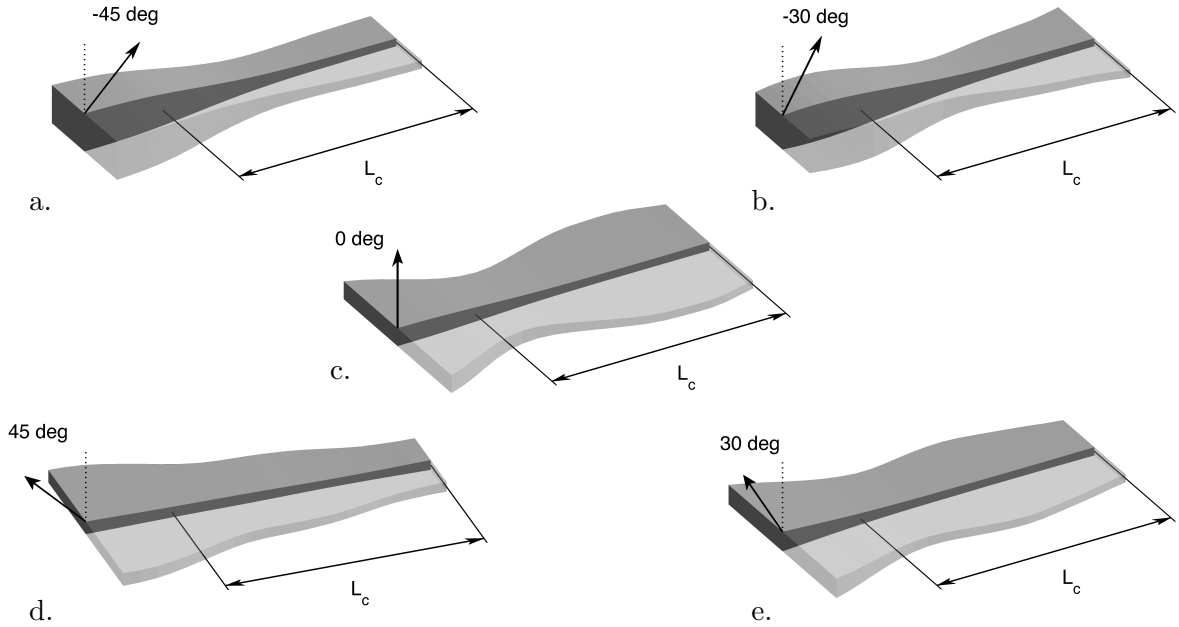


Figure 8: Optimum shapes obtained with computational shape optimization for Ψ_1 (single peeling direction), considering $\alpha \in [-45^\circ, 45^\circ]$, and $c_p = 1$, $c_c = 1$.

The peeling strip that we obtain for vertical peeling, $\alpha = 0^\circ$, resembles most closely the test geometry $(H_{\text{decr}}, B_{\text{const}})$, which is rated similarly to $(H_{\text{decr}}, B_{\text{decr}})$, see Figure 4c. For 30° and 45° , the strip tends to attain a small height but the maximum permitted width at the non-adhesive part. Table 3 shows the peeling force, the peak internal energy, and the contact energy for all geometries obtained here. Compared to all test geometries discussed in Section 3, the shapes obtained with the optimization procedure have a larger contact area and maximum force with acceptable maximum deformation, see Tables 1, 2, and 3. The total cost, Ψ_1 , is thus significantly smaller than for each of the best-rated test shapes, see Table 3 and Figure 4.

α	Ψ_1	$P_{\max}/P_{\max}^{\text{ref}}$	$\Pi_{\text{int}}^{\max}/\Pi_{\text{int}}^{\text{ref}}$	$\Pi_c^\infty/\Pi_c^{\text{ref}}$	V/V_{\max}
-45°	2.05	2.42	0.86	1.29	1.00
-30°	2.02	2.26	0.89	1.44	1.00
0°	1.73	2.11	0.83	2.35	0.88
30°	1.41	3.48	0.65	2.13	0.80
45°	1.38	5.68	0.64	1.78	0.69

Table 3: Normalized maximum peeling force, maximum internal energy, and total contact energy of the best-rated geometries obtained with computational shape optimization for the objective function Ψ_1 and $\alpha \in [-45^\circ, 45^\circ]$.

4.2 Combined peeling directions

We finally minimize $\Psi_2(\alpha_{\max}, \alpha_{\min})$ in Eq. (12) in order to obtain strongly adhesive peeling strips that can be detached easily for a certain peeling direction. The results are compared to those geometries obtained for a single direction, $\Psi_1(\alpha)$, see Section 4.1, where $\alpha = \alpha_{\max}$. Since we want to investigate how the additional requirement of easy detachment influences the strip shape, we also minimize the peeling force towards a single direction by considering

$$\Psi_1^*(\alpha) = c_p \bar{P}_{\max}(\alpha) + \bar{\Pi}_{\text{int}}^{\max}(\alpha) + \frac{c_c}{\bar{\Pi}_c^\infty}, \quad (17)$$

where $\alpha = \alpha_{\min}$. Figure 9 shows optimum geometries obtained for the three objective functions Ψ_1 , Ψ_2 , and Ψ_1^* and the peeling directions $\{\alpha_{\max}, \alpha_{\min}\} = \{45^\circ, -45^\circ\}$ and $\{30^\circ, -30^\circ\}$. We use the weightings $c_p^{\max}, c_p^{\min} \in \{1, 5\}$ and $c_p = c_c = 1$ here. The other parameters correspond to those of Section 4.1, see Table 7. The solid / dashed arrows in the figure indicate that P_{\max} is maximized / minimized towards this direction. Table 4 shows the maximum peeling forces of the geometries of Figure 9 for both directions, α_{\max} and α_{\min} . Depending on how strongly the requirement of easy detachment towards α_{\min} is weighted in Ψ_2 and Ψ_1^* the geometry tends to be very slender at its adhesive part. For the five cases considered here, the forces towards α_{\max} and α_{\min} become smallest for Ψ_2 with $c_p^{\max} = 1$, $c_p^{\min} = 5$, where the strip attains nearly the minimum permitted width along L . We note that we do not prescribe a minimum for the strip volume here. Differences between this shape and the geometry obtained for Ψ_1^* are reasonable because the weightings of the requirements concerning easy detachment, small deformation, and large contact energy are different. For $c_p^{\max} = 5$, $c_p^{\min} = 1$, the structure resembles slightly the shape obtained for Ψ_1 . In general, we observe a strong dependence of the shapes on the applied weightings.

As Table 4 shows, the ratio of $P_{\max}(\alpha_{\max})/P_{\max}(\alpha_{\min})$ is larger for larger differences in the peeling angles, $|\alpha_{\max} - \alpha_{\min}|$. In contrast to the geometries for the single peeling directions, Ψ_1 and Ψ_1^* , the strips obtained considering multiple directions incorporate both strong attachment towards α_{\max} but easy detachment towards α_{\min} , see Table 4.

5 Conclusion

This paper investigates optimal shapes of thin and flexible peeling strips for different peeling directions. We consider the maximum force, the strain energy due to elastic deformation, and the overall peeling energy as optimization criteria here. The peeling strip is modeled by using a finite beam element formulation of Sauer and Mergel [12], which is based on the geometrically exact beam theory of Reissner [9]. An exponential cohesive zone model of Xu and Needleman [17]

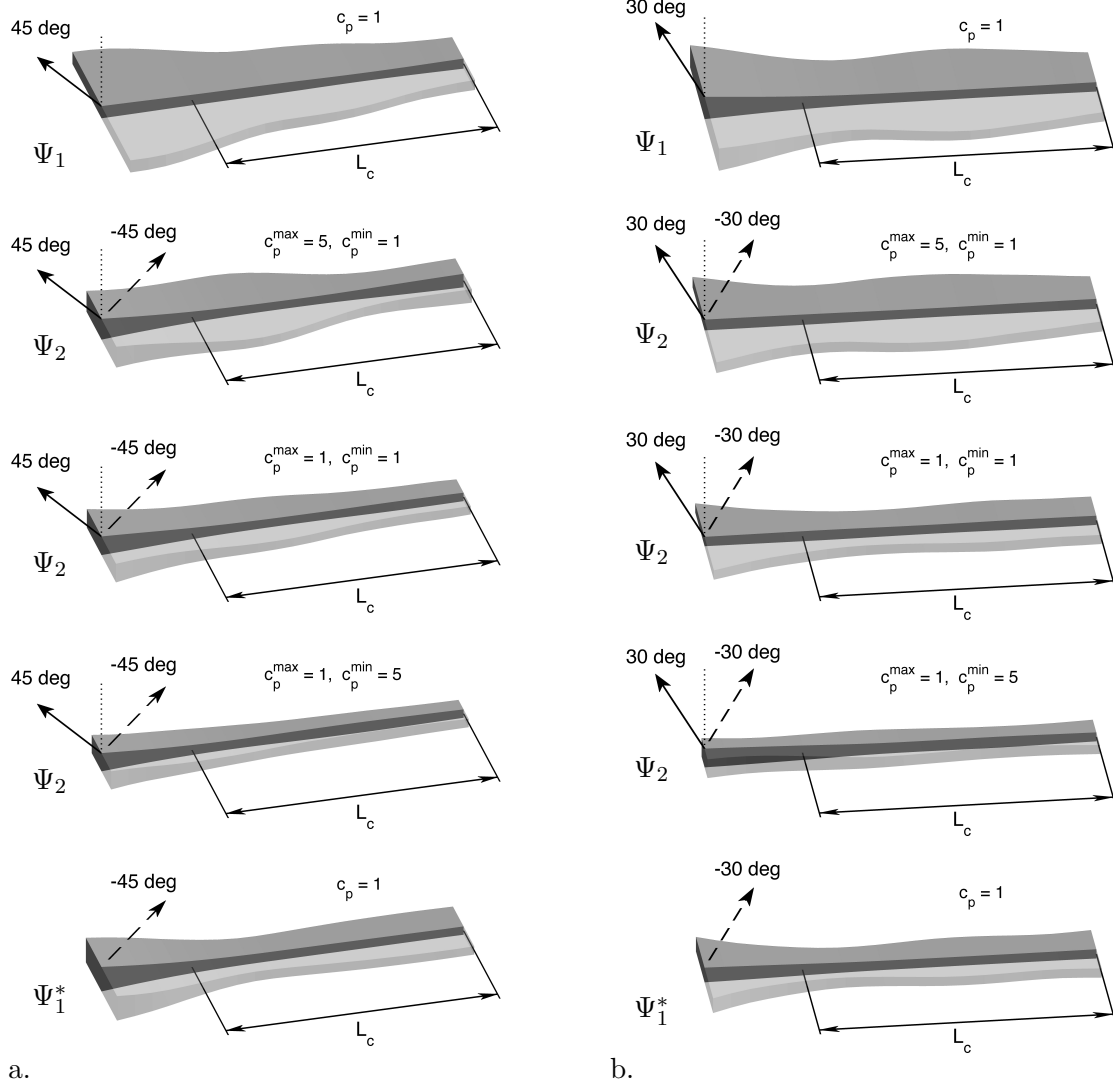


Figure 9: Geometries obtained with computational shape optimization for $\Psi_2(\alpha_{\max}, \alpha_{\min})$ (multiple peeling directions) compared to results for $\Psi_1(\alpha_{\max})$ and $\Psi_1^*(\alpha_{\min})$, considering $c_p^{\max}, c_p^{\min} \in \{1, 5\}$ and $c_p = c_c = 1$: a. Peeling direction $\{\alpha_{\max}, \alpha_{\min}\} = \{45^\circ, -45^\circ\}$; b. $\{\alpha_{\max}, \alpha_{\min}\} = \{30^\circ, -30^\circ\}$. The solid / dashed arrows indicate that P_{\max} is maximized / minimized towards this direction.

is considered to model the normal and tangential forces that act on the strip during the peeling process.

Two different cases are studied here:

1. Shape optimization for a single peeling angle, and
2. optimization by combining two different angles in order to obtain strong adhesion but easy detachment for different peeling directions.

Both are examined by accounting for a prescribed set of test geometries and by performing computational shape optimization. We use the optimization algorithm proposed by Mergel et al. [7] who consider the optimal shape of adhesive microstructures for peeling normal to the substrate.

$\{\alpha_{\max}, \alpha_{\min}\}$	Considered objective function	$\bar{P}_{\max}(\alpha_{\max})$	$\bar{P}_{\max}(\alpha_{\min})$	V/V_{\max}
$\{45^\circ, -45^\circ\}$	Ψ_1 ($c_p = 1$)	5.68	(1.02)	0.69
	Ψ_2 ($c_p^{\max} = 5, c_p^{\min} = 1$)	4.11	0.63	0.48
	Ψ_2 ($c_p^{\max} = 1, c_p^{\min} = 1$)	2.78	0.45	0.37
	Ψ_2 ($c_p^{\max} = 1, c_p^{\min} = 5$)	1.91	0.31	0.25
	Ψ_1^* ($c_p = 1$)	(2.68)	0.48	0.44
$\{30^\circ, -30^\circ\}$	Ψ_1 ($c_p = 1$)	3.48	(1.15)	0.80
	Ψ_2 ($c_p^{\max} = 5, c_p^{\min} = 1$)	2.88	0.97	0.53
	Ψ_2 ($c_p^{\max} = 1, c_p^{\min} = 1$)	1.82	0.65	0.34
	Ψ_2 ($c_p^{\max} = 1, c_p^{\min} = 5$)	1.08	0.34	0.24
	Ψ_1^* ($c_p = 1$)	(1.68)	0.58	0.34

Table 4: Maximum peeling forces towards α_{\max} and α_{\min} , considering the optimum geometries for $\Psi_1(\alpha_{\max})$, $\Psi_2(\alpha_{\max}, \alpha_{\min})$, $\Psi_1^*(\alpha_{\min})$ with $c_c = 1$, see Fig. 9.

We observe that the force required to initialize strip peeling depends strongly on the chosen peeling direction. The maximum can be observed for peeling parallel to the substrate, for which the strip is purely elongated. The peeling behavior in the opposite direction depends on the bending resistance of the considered strip. We recognize that both the strip height and width influence strongly the following peeling behavior of the strip. This influence can be increased by varying the peeling angle. One can thus not assume a priori that the maximum force occurs at the initialization of the peeling process. The geometries that we obtain with computational shape optimization for multiple peeling directions differ in both the shape and the peeling behavior from those considering a single peeling direction. Depending on the weighting of the considered criteria, these peeling strips are less adhesive but can be detached more easily for a prescribed direction. In conclusion, the optimum shape of the thin strip may depend on many other parameters, such as the length of its adhesive part or its total length compared to the range of adhesion [7]. A study varying all weighting, geometry, and adhesion parameters would thus be of further interest.

A Parameters

This section provides the parameters used for the results in Sections 3 and 4. All parameters are normalized with Young's modulus, E , and a unit length, L_0 .

geometry	$L = 200 L_0, \quad c_B = 40 L_0, \quad d_B = 0.2, \quad c_H = 12 L_0 + \Delta c_H, \quad d_H = 0.06,$ choose Δc_H s.t. $V = 9.6 \cdot 10^4 L_0^3$
material	$E, \quad \nu = 0.2, \quad G = E / [2(1 + \nu)]$
cohesion	$T_0 = 0.3088 E, \quad g_0 = 0.0913 L_0, \quad \varepsilon = 50 E / L_0^2, \quad L_c = 0.75 L$

Table 5: Parameters for the test geometries investigated in Section 3.

$P_{\max}^{\text{ref}} [E L_0^2]$	$\Pi_{\text{int}}^{\text{ref}} [E L_0^3]$	$\Pi_c^{\text{ref}} [E L_0^3]$
3.99	76.91	459.90

Table 6: Normalization quantities obtained with geometry ($H_{\text{const}}, B_{\text{const}}$): Maximum peeling force, peak internal energy, and total contact energy.

geometry	$L = 200 L_0$, $V_{\max} = 1.5 \cdot 10^5 L_0^3$, $H''_{\max} = 0.05 / L_0$, $B''_{\max} = 0.35 / L_0$ $H_{\min} = 5 L_0$, $H_{\max} = 25 L_0$, $B_{\min} = 15 L_0$, $B_{\max} = 120 L_0$
material	E , $\nu = 0.2$, $G = E / [2(1 + \nu)]$
cohesion	$T_0 = 0.3088 E$, $g_0 = 0.0913 L_0$, $\varepsilon = 50 E / L_0^2$, $L_c = 0.75 L$
optimization	$N_{\text{total}} = 80$, $N_{\text{child}} = 18$, $N_{\text{new}} = 24$, $N_{\text{mutate}} = 4$, $n_{\text{el}}^{\text{op}} = 20$, $\mu_{\text{abs}} = 0.05$, $\mu_{\text{rel}} = 0.25$, $\mu = 0.01$, see [7]

Table 7: Parameters for the shape optimization discussed in Section 4.

Acknowledgements

The authors are grateful to the German Research Foundation (DFG) for supporting this research under project SA1822/5-1 and GSC111.

References

- [1] K. Autumn, A. Dittmore, D. Santos, M. Spenko, and M. Cutkosky. Frictional adhesion: A new angle on gecko attachment. *J. Exp. Biol.*, 209:3569–3579, 2006.
- [2] K. Autumn, Y. A. Liang, S. T. Hsieh, W. Zesch, W. P. Chan, T. W. Kenny, R. Fearing, and R. J. Full. Adhesive force of a single gecko foot-hair. *Nature*, 405:681–685, 2000.
- [3] B. Chen, P. Wu, and H. Gao. Pre-tension generates strongly reversible adhesion of a spatula pad on substrate. *J. R. Soc. Interface*, 6:529–537, 2009.
- [4] B. Chen, P. D. Wu, and H. Gao. Hierarchical modelling of attachment and detachment mechanisms of gecko toe adhesion. *Proc. R. Soc. A*, 464:1639–1652, 2008.
- [5] C. Greiner, R. Spolenak, and E. Arzt. Adhesion design maps for fibrillar adhesives: The effect of shape. *Acta Biomater.*, 5:597–606, 2009.
- [6] K. Kendall. Thin-film peeling – the elastic term. *J. Phys. D: Appl. Phys.*, 8:1449–1452, 1975.
- [7] J. C. Mergel, R. A. Sauer, and A. Saxena. Computational optimization of adhesive microstructures based on a nonlinear beam formulation. *Struct. Multidiscip. Optim.*, 2013. Under revision.
- [8] A. Pantano, N. M. Pugno, and S. N. Gorb. Numerical simulations demonstrate that the double tapering of the spatulae of lizards and insects maximize both detachment resistance and stability. *Int. J. Fract.*, 171:169–175, 2011.
- [9] E. Reissner. On one-dimensional finite-strain beam theory: The plane problem. *J. Appl. Math. Phys.*, 23:795–804, 1972.
- [10] R. A. Sauer. The peeling behavior of thin films with finite bending stiffness and the implications on gecko adhesion. *J. Adhes.*, 87(7-8):624–643, 2011.
- [11] R. A. Sauer and L. De Lorenzis. A computational contact formulation based on surface potentials. *Comput. Meth. Appl. Mech. Eng.*, 253:369–395, 2013.

- [12] R. A. Sauer and J. C. Mergel. A geometrically exact finite beam element formulation for thin film adhesion and debonding. *Finite Elem. Anal. Des.*, 2013. Under revision.
- [13] R. Spolenak, S. Gorb, and E. Arzt. Adhesion design maps for bio-inspired attachment systems. *Acta Biomater.*, 1:5–13, 2005.
- [14] R. Spolenak, S. Gorb, H. Gao, and E. Arzt. Effects of contact shape on the scaling of biological attachments. *Proc. R. Soc. A*, 461:305–319, 2005.
- [15] K. Sylves, K. Maute, and M. L. Dunn. Adhesive surface design using topology optimization. *Struct. Multidiscip. Optim.*, 38:455–468, 2009.
- [16] Y. Tian, N. Pesika, H. Zeng, K. Rosenberg, B. Zhao, P. McGuiggan, K. Autumn, and J. Israelachvili. Adhesion and friction in gecko toe attachment and detachment. *Proc. Natl. Acad. Sci. U.S.A.*, 103(51):19320–19325, 2006.
- [17] X.-P. Xu and A. Needleman. Void nucleation by inclusion debonding in a crystal matrix. *Modelling Simul. Mater. Sci. Eng.*, 1:111–132, 1993.
- [18] B. Zhao, N. Pesika, K. Rosenberg, Y. Tian, H. Zeng, P. McGuiggan, K. Autumn, and J. Israelachvili. Adhesion and friction force coupling of gecko setal arrays: Implications for structured adhesive surfaces. *Langmuir*, 24:1517–1524, 2008.
- [19] B. Zhao, N. Pesika, H. Zeng, Z. Wei, Y. Chen, K. Autumn, K. Turner, and J. Israelachvili. Role of tilted adhesion fibrils (setae) in the adhesion and locomotion of gecko-like systems. *J. Phys. Chem. B*, 113:3615–3621, 2009.